Contrib Mineral Petrol (2002) 143: 551–566
DOI 10.1007/s00410-002-0366-5

S. Jung · S. Hoernes · K. Mezger

Synorogenic melting of mafic lower crust: constraints from geochronology, petrology and Sr, Nd, Pb and O isotope geochemistry of quartz diorites (Damara orogen, Namibia)

Received: 12 December 2001 / Accepted: 8 April 2002 / Published online: 20 June 2002

Abstract Quartz diorites represent the earliest (ca. 540 Ma) and most primitive plutonic rocks in the Pan African Damara belt and they pre-date the main phase of high-T regional metamorphism. Two suites of synorogenic quartz diorites are unusual among Damaran intrusive rocks in their elemental and isotopic features. Comparison of the diorite compositions with melts from amphibolite-dehydration melting experiments points to a garnet-bearing meta-tholeiite, probably enriched in K_2O, as a likely source rock. Partial melting processes generated mafic (ca. 50 wt% SiO_2) quartz diorites in the deep crust at temperatures of between 1,000 and 1,100 °C, based on comparison with experimental results and similar temperature estimates based on P_2O_5 solubility in mafic rocks. Subsequently, the quartz diorites evolved by multistage, polybaric differentiation processes including fractional crystallization of mainly hornblende and plagioclase and assimilation of felsic basement gneisses. Although their chemical characteristics (high LILE, low HFSE) resemble those of other quartz diorites with calc-alkaline affinities, they differ in their enriched Sr (initial $^{87}Sr/^{86}Sr$: 0.70943–0.71285), Nd (initial ϵ Nd: –9.1 to –15.2) and O ($\delta^{18}O$: 6.8–8.1‰) isotope compositions. Neodymium model ages (T_{DM}) that range from 1.7 to 2.2 Ga and large variation in $^{207}Pb/^{204}Pb$ relative to $^{206}Pb/^{204}Pb$ indicates involvement of ancient crustal material. Lead ($^{206}Pb/^{204}Pb$: 17.08–17.23, $^{207}Pb/^{204}Pb$: 15.53–15.62, $^{208}Pb/^{204}Pb$: 37.71–38.16) isotope compositions are strongly retarded, indicating that the source underwent a pre-Pan-African U/Pb fractionation and U depletion. It is proposed that the quartz diorites originated by synorogenic high temperature melting of mafic lower crust. This contrasts with previous suggestions favouring an origin of these rocks by melting of an enriched mantle during Pan-African times with characteristics modified by subduction of oceanic crust and sedimentary rocks.

S. Jung (✉)
Max-Planck-Institut für Chemie,
Abt. Geochemie, Postfach 3060,
55020 Mainz, Germany
E-mail: sjung@mpch-mainz.mpg.de
Fax: +49-6131-371051

S. Hoernes
Mineralogisch-Petrologisches Institut der Universität Bonn,
Poppelsdorfer Schloß,
53115 Bonn, Germany

K. Mezger
Universität Münster,
Institut für Mineralogie,
Corrensstr. 24, 48149
Münster, Germany

Editorial responsibility: J. Hoefs

Introduction

Granite batholiths are an important and characteristic component of continental crust. They form from granitic melts that are often not primary melts, but are modified by differentiation processes prior to emplacement and crystallization. The relative importance of fractional crystallization versus partial melting and the role of open system processes (magma mixing, assimilation) in the genesis of these differentiated melts is still being debated. In areas where granite batholiths consist not only of granites sensu stricto, but also of more mafic rocks (gabbros, diorites), a fundamental role has been assigned to these mafic magmas. In general, they may be mantle-derived parental magmas (LeBel et al. 1985), end members in mixing and fractionation-assimilation processes (DePaolo 1981; Reid et al. 1983; Kistler et al. 1986; Eggins and Hensen 1987), material from lower crustal source regions (Gromet and Silver 1987; Tepper et al. 1993) and/or heat sources that drive melting of overlying continental crust (Pitcher 1987). Additionally, their petrological diversity can also be the result of source heterogeneity (Noyes et al. 1983).

Granitoid intrusions are an important rock type throughout the Damara Belt (Namibia). Chemical and isotopic data accumulated in recent years indicate that

these granitoids consist of several distinct suites. These suites include (1) synorogenic S-type granites that originated by partial melting of upper crustal metasedimentary rocks (Haack et al. 1982; McDermott et al. 1996; Jung et al. 2000a, 2001), (2) synorogenic granites that were derived by melting of undepleted metasedimentary and meta-igneous basement rocks (McDermott et al. 1996; Jung et al. 2002) and (3) late-orogenic A-type granites, some of them represent mixtures between moderately depleted meta-igneous source rocks and a component from the lithospheric mantle (Jung et al. 1998b). One objective of this study is to unravel the petrogenesis of synorogenic dioritic intrusions.

High-precision Sm–Nd and Pb–Pb (garnet, zircon) and U–Pb ages (monazite, titanite) are now available from a number of migmatite and granite occurrences throughout the high-grade central part of the Pan-African Damara orogen of Namibia (Briqueu et al. 1980; Kukla et al. 1991; Jung et al. 1998b, 2000a, 2000b, 2001; Jung and Mezger 2001, 2002). These ages provide a temporal framework for the structural and petrological evolution of the orogen. Thus, another objective of this study is to determine the temporal relationships between the time of intrusion of the quartz diorites as constrained by new high-precision U–Pb titanite ages relative to the time of high-grade metamorphism and melting. This comparison is particularly relevant for the quartz diorites because they may represent an important thermal component during orogeny.

The Damara Belt is interpreted to have formed mainly by continental collision including subduction, although the significance of the ocean floor involved in the orogeny is still a matter of debate (Kröner 1982; Miller 1983). In contrast to many typical collision belts (e.g. Caledonides, Alps), the Damara Belt is characterized by the emplacement of large volumes of granitoids similar to that observed in some active continental margins (e.g. Andes) or in broad ensialic orogens (e.g. Lachlan Fold belt). However, the general pattern of the Damaran plutonism contrasts with Cordilleran-type plutonism, both in its spatial distribution and bulk chemistry. In the Damara orogen, the proportions of gabbro:diorite–granodiorite:tonalite–granite:leucogranite contrast markedly with those found in continental margin environments. In the Andes, the proportions of gabbro:diorite–granodiorite:tonalite-granite are 16:58:26 (Pitcher 1978), whereas in the Damara Belt the proportions are 2:2:96 (Miller 1983), broadly similar to the proportions found in the Himalayas (0:0:100; Le Fort et al. 1987). Furthermore, the plutonic rocks in the Damara orogen are not arranged in linear belts, and leucocratic rocks are far more abundant than in subduction zone settings. Hawkesworth and Marlow (1983) have, based on trace element arguments, questioned the derivation of most Damaran granites from a subduction zone. Nonetheless, several workers (Kasch 1983; Miller 1983) have suggested that the Pan-African orogeny, and hence the associated plutonism of the Damara orogen of Namibia, is related to subduction zone processes. The paucity of geological evidence for a fossil subduction zone, e.g. the lack of eclogites and blueschists indicating a high P–low T regime casts some doubts on this hypothesis and alternative models involving ensialic tectonism have been proposed (e.g. Kröner 1982). Because Kasch (1983) and Miller (1983) used the occurrence of quartz diorites and associated granodiorites and granites in the southern central Zone of the Damara Belt (Fig. 1) as an argument for a subduction zone setting, an evaluation of the isotope systematics of these rocks highlights the relative importance assigned to the mantle or to the crust for melt production during orogeny. Such an isotope study can provide valuable constraints on the relative role of crustal recycling and new mantle additions to the continental crust during orogenic processes.

Analytical techniques

Whole rock powders were prepared using a jaw crusher, a ball mill and an agate mortar. Major and some trace elements (except for REE) were determined on fused lithium-tetraborate glass beads using standard XRF techniques. Rare earth elements were analysed by inductively coupled plasma emission spectrometry following separation of the matrix elements by ion exchange (Heinrichs and Herrmann 1990). Loss on ignition (LOI) was determined gravimetrically after heating the samples at 1,050 °C for 1 h (Lechler and Desilets 1987). FeO was measured titrimetrically with standard techniques. Accuracy has been controlled by repeated measurements against several international and in-house standards.

For the Rb–Sr and Sm–Nd whole rock isotope analyses, the samples were spiked with a $^{149}Sm/^{150}Nd$ and a $^{85}Rb/^{84}Sr$ tracer and digested in concentrated HF-HNO_3 in 3-ml screw-top Teflon vials inside Krogh-style Teflon bombs at 200 °C for 3 days. After complete dissolution, the samples were dried down and redissolved in 2.5 N HCl. Rb, Sr and REE were separated by using standard cation exchange columns with a Dowex AG 50 W-X 12 resin using 2.5 N HCl for Rb and Sr and 6 N HCl for the REE. Nd and Sm were separated from the other REE by using HDEHP-coated Teflon columns and 0.12 N HCl for Nd and 0.3 N HCl for Sm. Isotope analyses were carried out at the Max-Planck-Institut für Chemie at Mainz using thermal ionization mass spectrometry with a Finnigan MAT 261 multicollector mass spectrometer operating in the static mode. Rb, Sm and Nd were run on Re double filaments and Sr was run on W single filaments. Nd isotopes were normalized to $^{146}Nd/^{144}Nd = 0.7219$. The total procedural blank for Nd was < 40 pg and is considered to be negligible. Repeated measurements of the La Jolla Nd standard gave $^{143}Nd/^{144}Nd = 0.511854 \pm 0.000031$ (2σ; $n = 24$). The reproducibility of the Sr standard (NBS 987) is $^{87}Sr/^{86}Sr = 0.710218 \pm 0.000029$ (2σ; $n = 24$) and the fractionation was corrected to $^{86}Sr/^{88}Sr$: 0.1194. Uncertainties in the $^{87}Sr/^{86}Sr$ and $^{143}Nd/^{144}Nd$ are reported in the last two digits. Typical analytical errors in the $^{87}Rb/^{86}Sr$ and $^{147}Sm/^{144}Nd$ ratios are equal or better than 0.5 and 0.1%, respectively. Between 30 and 50 mg of high-purity K-feldspar separates were washed with a mixture of 3:1 HCl/HNO_3 to remove surface contamination and were subsequently rinsed three times with ultrapure water. After this treatment, the separates were leached three times in a mixture of concentrated HF/HNO_3, which resulted in a weight loss of ~70–80%. Subsequently, the feldspars were dissolved in concentrated HF and after evaporation redissolved in 2.5 N HCl and 0.6 N HBr and loaded on Teflon columns filled with Dowex AG 1 X 8 anion exchange resin (100–200 mesh) in chloride form (Mattinson 1986). The Pb was extracted using conventional HBr/HCl techniques and was loaded on Re single filaments following the H_3PO_4-silica gel method (Cameron et al. 1969). Pb analyses were corrected for mass fractionation by a factor of 0.11%

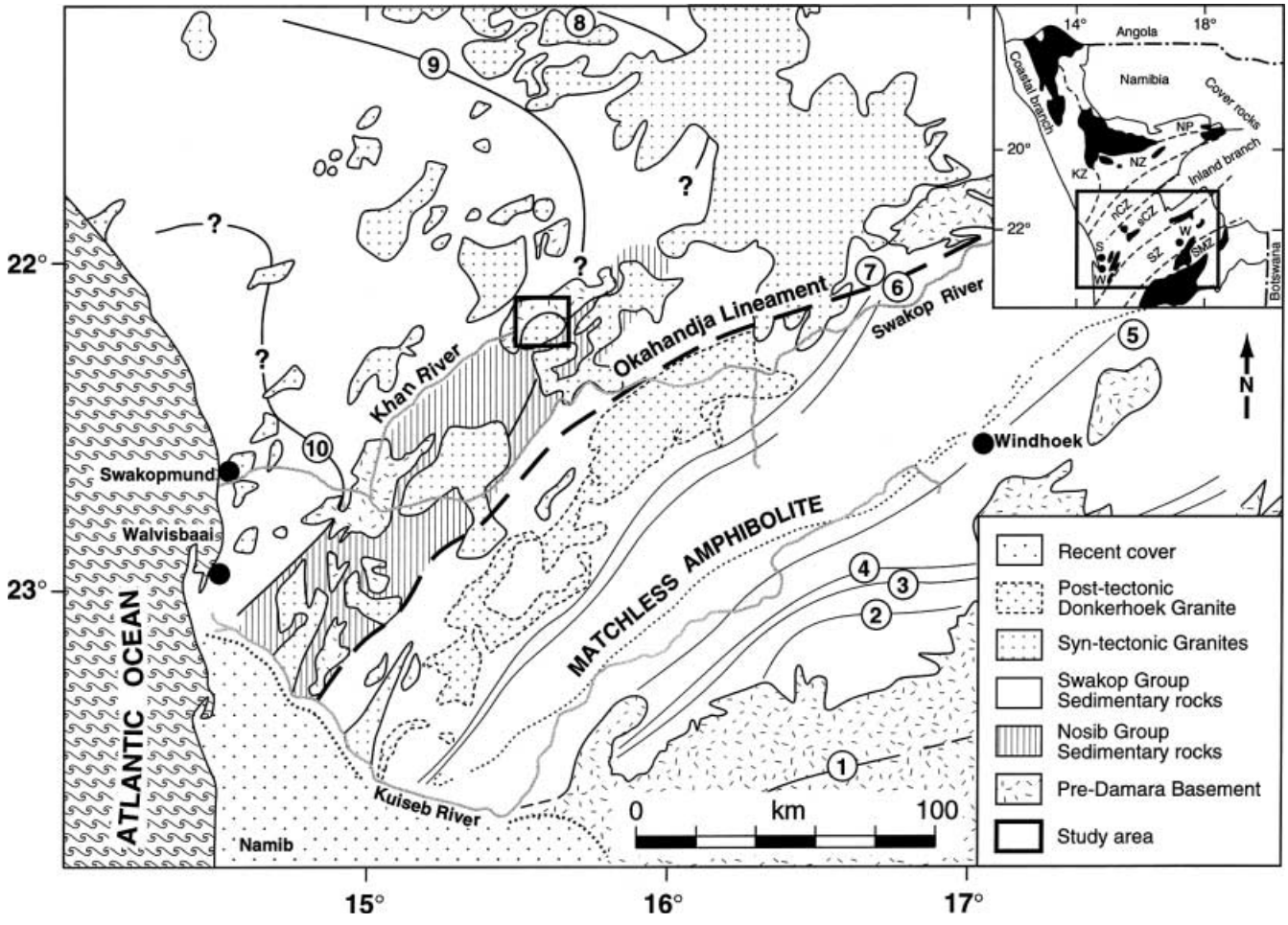

Fig. 1. Generalized geological map showing the study area within the Central Zone of the Damara orogen, Namibia. *Abbreviations* in *inset*: *KZ* Kaoko Zone; *NP* Northern Platform; *NZ* Northern Zone; *nCZ* northern Central Zone; *sCZ* southern Central Zone; *SZ* Southern Zone; *SMZ* Southern Margin Zone. Isograd map (Hartmann et al. 1983) gives the distribution of regional metamorphic isograds within the southern and central Damara orogen. Isograds: (*1*) biotite-in, (*2*) garnet-in, (*3*) staurolite-in, (*4*) kyanite-in, (*5*) cordierite-in, (*6*) andalusite–sillimanite, (*7*) sillimanite-in according to staurolite-breakdown, (*8*) partial melting because of muscovite + plagioclase + quartz + $H_2O \leftrightarrow$ melt + sillimanite, (*9*) K-feldspar + cordierite-in, (*10*) partial melting because of biotite + K-feldspar + plagioclase + quartz $\leftrightarrow$ cordierite–melt + garnet. *W* Walvisbay; *S* Swakopmund; *Wh* Windhoek

per amu. The reproducibility of the standard NBS 982 was estimated to be 0.068, 0.064 and 0.071% for the $^{206}Pb/^{204}Pb$, $^{207}Pb/^{204}Pb$ and $^{208}Pb/^{204}Pb$ ratio, respectively. The total procedure blank was <100 pg Pb and, therefore, was, considered negligible.

After sieving the samples through a 40–80-mesh fraction, the mineral separates were purified by magnetic separation, separated by methylene iodide and handpicked, which produced high-purity separates. Only minerals free of inclusions were used. The titanites were washed in warm deionized water to remove surface contamination and were spiked with a $^{205}Pb/^{235}U$ spike before digesting in concentrated HF/HNO_3 in 3-ml screw-top Teflon vials inside Krogh-style Teflon bombs at 200 °C for several days. The titanites were boiled three times in 7 N HNO_3 and were subsequently dissolved in 3 N HCl for ion exchange chromatography. The Pb was separated using HCl–HBr chemistry and the U was separated using Eichrome resin and an improved 2 N HNO_3/0.02 N HNO_3 chemistry. Lead isotope analyses were carried out as described above. Low U concentrations, combined with elevated common Pb concentrations, result in rather large uncertainties for the analyses. In order to correct for initial Pb composition, the Pb composition of leached K-feldspar from each sample was measured and was taken as the initial Pb composition during titanite growth.

Oxygen isotope analyses were performed at the University of Bonn on ~10-mg aliquots of powdered whole-rock samples, using purified fluorine for oxygen extraction, followed by conversion to CO_2 (Clayton and Mayeda 1963). $^{18}O/^{16}O$ measurements were made on a SIRA-9 triple-collector mass spectrometer by VG-Isogas. Analytical uncertainties are $<0.2‰$.

Geological setting and rock types

The Damara orogen exposes a deeply eroded section through a Pan African mobile belt that can be divided into a N–S-trending coastal branch, the Kaoko belt, and a NE–SW-trending intracontinental branch (see inset to Fig. 1). This mobile belt has been divided into several zones based mainly on stratigraphy, metamorphic grade, structure and geochronology (Miller 1983). The Central Zone is characterized by a large number of granitoids that record mineral and Rb/Sr whole rock ages mostly between 650 and 460 Ma and outcrop over an area of approximately 75.000 km^2 (Miller 1983; Fig. 1). Pre-Damara basement gneisses are overlain by Neoproterozoic to Palaeozoic metasedimentary sequences

comprising quartzose sandstones, arkoses, mica schists, calc-silicate rocks, marble, metamorphosed glaciogenic diamictites, banded iron-stones, Al-rich metapelites, migmatites, metacarbonates and conglomerates (Miller 1983).

In the Central Zone (Fig. 1), previous estimates for the peak metamorphic temperatures are 560–650 °C at 3 ± 1 kbar for impure marbles (Puhan 1983). Metamorphic conditions based on oxygen isotope fractionation in a variety of meta-sedimentary and meta-igneous rocks yielded similar temperature estimates of 570–650 °C (Hoernes and Hoffer 1979). The metamorphic grade increases from east to west reaching high-grade conditions with local partial melting in the coastal area (Hartmann et al. 1983). However, more recent results indicated high-grade conditions that culminated in medium-pressure high-temperature granulite facies conditions with temperatures estimated to have been in excess of 700 °C at 4–6 kbar (Masberg et al. 1992; Jung et al. 1998c, 2000b; Jung and Mezger 2002). To the south-east, there is a gradation into the Okahandja Lineament Zone that separates the Central Zone from the Southern Zone (Fig. 1). In the Southern Zone, regional metamorphism is characterized by a Barrovian-type sequence with a general increase in the metamorphic grade from south to north. The metamorphic conditions range from low to medium pressures, and reached up to 8 kbar at maximum temperatures of 600 °C. Intrusions of large granitic bodies are absent even in the highest grade zone.

Important bodies of quartz diorites are exposed in the Goas (15.50°E/22.15°S) and Okongava (15.55°E/22.00°S) areas, which are located within the southern Central Zone (Fig. 1). Additional intrusions of quartz diorite include the nearby Palmental diorite (15.50°E/22.20°S) and the Mon Repos diorite (15.45°E722.05°S) both of which are not treated in this study. Plutons in the Goas and Okongava area are unzoned and range from quartz diorite through granite; leucogranites are less abundant. The plutonic rocks are generally medium grained, equigranular and hypidiomorphic with 50–70% plagioclase, 10–20% each hornblende and biotite, 5–15% quartz and 10–20% K-feldspar. Hornblende and plagioclase are the earliest-formed minerals and are virtually unzoned. Subhedral to anhedral hornblende can have rare inclusion of relict clinopyroxene and is usually associated with titanite and opaque minerals. Biotite may replace hornblende, quartz and K-feldspar occur mostly as interstitial phases. Accessory minerals include titanite, apatite, opaque minerals and zircon, in order of decreasing abundances. Alteration is weak or absent. Minor amounts of secondary minerals include mostly chlorite, muscovite and haematite. Enclaves of metasedimentary country rocks or other igneous rocks are absent.

Geochronology

In slowly cooled high-grade metamorphic terranes, U–Pb titanite ages are generally interpreted as dating the time of cooling through the closure temperature for Pb volume diffusion (T_c). Estimates of T_c based on slowly cooled natural samples with a small grain size are ca. 600 °C (Tucker et al. 1986; Heaman and Parrish 1991) or 660–700 °C (Mezger et al. 1993; Scott and St-Onge 1995). Experimentally determined Pb diffusion parameters (Cherniak 1993) indicate a closure temperature for a grain size of ca. 200 μm of ca. 630 °C for a cooling rate of 10 °C/Ma and ca. 600 °C for a cooling rate of 2 °C/Ma. Recent studies provide evidence that an inherited Pb component can be preserved in titanite incorporated into syenite melts (Pidgeon et al. 1996; Zhang and Schärer 1996). This indicates T_c in excess of 710 °C for titanite, but only for very short-lived magmatic events. In slowly cooled high-grade metamorphic terranes titanite ages probably date cooling during the waning stages of metamorphism (Mezger et al. 1991), whereas in short-lived igneous bodies U–Pb titanite ages can provide prograde ages that constrain the time of intrusion (Verts et al. 1996).

Titanite was recovered from both quartz diorites at Goas and Okongava. Dark brown titanite grains were generally sub-spherical, anhedral to euhedral and 100 to 500 μm in diameter. All selected fractions were free of visible inclusions. Most U–Pb analyses of titanite samples from Goas are concordant with $^{207}Pb/^{206}Pb$ ages of between 533 ± 4 and 538 ± 2 Ma (Tables 1 and 2, Fig. 2). One sample is normally discordant and yielded a similar $^{207}Pb/^{206}Pb$ age of 533 ± 3 Ma. One sample yielded a younger $^{207}Pb/^{206}Pb$ age of 503 ± 3 Ma. Most titanite fractions extracted from quartz diorites from Okongava are concordant, with $^{207}Pb/^{206}Pb$ ages of between 524 ± 2 and 557 ± 1 Ma. Normal discordant titanites yielded $^{207}Pb/^{206}Pb$ ages between 538 ± 2 and 551 ± 1 Ma. One fraction gave an apparently older $^{207}Pb/^{206}Pb$ age of 579 ± 4 Ma, whereas another fraction yielded a younger $^{207}Pb/^{206}Pb$ age of 520 ± 2 Ma. A regression line through all samples in $^{206}Pb/^{204}Pb$ versus $^{207}Pb/^{204}Pb$ space yielded a $^{207}Pb/^{206}Pb$ age of 551.9 ± 0.7 Ma.

Geochemistry

Major and trace elements

The quartz diorites have SiO_2 concentrations between 56.3 and 61.8 wt% (Goas) and between 51.6 and 59.5 wt% (Okongava) (Tables 3 and 4). All samples are metaluminous with alumina saturation index [ASI; = molar A/CNK: $(Al_2O_3/CaO + Na_2O + K_2O)$] values ranging from 0.88 to 1.01 at Goas and from 0.79 to 0.92 at Okongava. Mafic samples have $K_2O < Na_2O$, whereas more evolved samples have $K_2O > Na_2O$. There is a large variation in MgO, TiO_2, FeO_{total}, CaO, Al_2O_3 and K_2O among both suites of quartz diorites in which MgO, TiO_2, FeO_{total}, CaO, Al_2O_3 and P_2O_5 decrease and K_2O increases with increasing SiO_2 (Fig. 3). The decrease in Al_2O_3 is more pronounced in samples from Okongava than in samples from Goas. Similarly,

Table 1. U–Pb titanite data from quartz diorites from the Damara orogen (Namibia). For analytical details see Analytical techniques

Sample name	Tnt M20	Tnt M21	Tnt M22	Tnt M24	Tnt M27	Tnt M29	Tnt M31	Tnt M33.1	Tnt M33.2
U (ppm)	143.0	138.1	134.0	297.4	312.6	227.7	142.2	411.6	340.9
Pb (ppm)	21.9	21.7	20.1	43.2	44.1	29.6	18.2	41.2	81.4
$^{206}Pb/^{204}Pb$	169.6	176.1	193.4	93.2	105.8	185.0	169.9	474.3	69.3
$^{208}Pb/^{206}Pb$	0.48113	0.53946	0.49757	0.14724	0.13825	0.22397	0.14658	0.61807	0.59990
$^{207}Pb/^{206}Pb$	0.057661	0.058170	0.058138	0.058081	0.057303	0.058228	0.057845	0.058348	0.059319
Error (%)	0.7759	0.2624	0.2451	0.5267	0.4564	0.2790	0.3367	0.7023	0.7162
$^{207}Pb/^{235}U$	0.70361	0.71440	0.71056	0.62901	0.64623	0.70831	0.70993	0.50981	0.74548
Error (%)	1.1173	1.7544	1.7488	1.8593	1.8216	1.7671	1.7631	2.1307	1.9333
$^{206}Pb/^{238}U$	0.08850	0.08907	0.08864	0.07855	0.08179	0.08822	0.08901	0.06337	0.09115
Error (%)	0.7538	1.7330	1.7300	1.7756	1.7579	1.7427	1.7272	1.9950	1.7818
$^{206}Pb/^{238}U$ age (million years)	547	550	548	487	507	545	550	396	562
$^{207}Pb/^{235}U$ age (million years)	541	547	545	495	506	544	545	418	566
$^{207}Pb/^{206}U$ age (million years)	517	536	535	533	503	538	524	543	579

trace element abundances of V, Cr, Ni, Zr, Y and Sr decrease with increasing SiO_2 (Fig. 4). Again, for samples from Okongava, the decrease in Sr is more pronounced than in samples from Goas. Rubidium and Th increase with increasing SiO_2. Barium shows a different behaviour. In samples from Okongava, Ba first increases between ca. 52 and 57 wt% SiO_2 and then decreases from 57 to 60 wt% SiO_2 whereas in samples from Goas, Ba decreases from 56 to 62 wt% SiO_2. For both suites of quartz diorites, rare earth elements (REE) are enriched with chondrite-normalized La abundances of between 129 and 184 (Goas) and between 95 and 222 (Okongava). Chrondrite-normalized Lu abundances are similar in both suites and range from 7.6 to 12.4 (Fig. 5). Both suites of quartz diorites show no Eu anomaly in the mafic rock types. With increasing SiO_2, negative Eu anomalies develop with maximum Eu/Eu* values of 0.67 for Goas and 0.60 for Okongava. Chondrite-normalized La_n/Yb_n ratios and Rb, Zr and Nb concentrations are similar to most crust-derived granites from the Damara orogen (McDermott et al. 1996; Jung et al. 1998b), but are higher than in quartz diorites derived from an upper mantle modified by a subduction zone component (e.g. Shaw et al. 1993).

Strontium, Nd, Pb and O isotopes

The results of the Sr, Nd, Pb and O isotope analyses are reported in Table 5. The quartz diorites at Goas have an unradiogenic Nd isotopic composition with initial ϵ_{Nd} values ranging from –12.8 to –14.6 and initial $^{87}Sr/^{86}Sr$ ratios ranging from 0.71081 to 0.71285. Quartz diorites from Okongava have a larger spread in Nd isotopic composition, with initial ϵ_{Nd} values ranging from –9.1 to –15.2. Initial $^{87}Sr/^{86}Sr$ ratios have values between 0.70943 and 0.71251 (Fig. 6). For both suites, initial ϵ_{Nd} values become less radiogenic and Sr isotope compositions become more radiogenic with decreasing MgO and increasing SiO_2.

The leached feldspars from Goas have $^{206}Pb/^{204}Pb$ ratios that range from 17.16 to 17.23 and $^{207}Pb/^{204}Pb$ ratios ranging from 15.53 to 15.56 (Fig. 7; Table 5). At Okongava, $^{206}Pb/^{204}Pb$ ratios are less radiogenic ranging from 17.08 to 17.17, but $^{207}Pb/^{204}Pb$ ratios are more radiogenic with values between 15.56 and 15.63. The $^{208}Pb/^{204}Pb$ ratios show considerable overlap with ratios from 37.71–37.90 at Goas and from 37.78–38.16 at Okongava. In $^{207}Pb/^{204}Pb$ vs. $^{206}Pb/^{204}Pb$ space both suites plot above the Pb evolution curve of Stacey and Kramers (1975; Fig. 7a) indicating strongly retarded Pb isotope compositions. In the $^{208}Pb/^{204}Pb$ vs $^{206}Pb/^{204}Pb$ diagram the samples plot above the Th/U evolution curve (Fig. 7b). Like the Nd and Sr isotope composition, $^{207}Pb/^{204}Pb$ and $^{208}Pb/^{204}Pb$ ratios show some variation with major element composition in which the Pb isotope ratios decrease with decreasing MgO for both suites. Similarly, for both suites, $^{207}Pb/^{204}Pb$ ratios decrease

Table 2. U–Pb titanite data from quartz diorites from the Damara orogen (Namibia). For analytical details see Analytical techniques

Sample name	Tnt M34.1	Tnt M34.2	Tnt M35.1	Tnt M35.2	Tnt M38.1	Tnt M38.2	Tnt M39.1	Tnt M39.2
U (ppm)	339.9	274.4	322.5	429.3	265.3	265.5	225.1	185.5
Pb (ppm)	37.7	50.3	43.0	75.4	39.2	55.2	40.9	58.5
$^{206}Pb/^{204}Pb$	438.5	140.4	565.6	139.5	414.9	146.8	243.6	70.3
$^{208}Pb/^{206}Pb$	0.80147	0.78730	0.62360	0.63276	1.02569	1.01996	1.60322	1.69092
$^{207}Pb/^{206}Pb$	0.058564	0.057746	0.058738	0.058279	0.0582095	0.0585063	0.0584058	0.0585126
Error (%)	0.3469	0.3533	0.2182	0.3548	0.2555	0.3223	0.4101	0.8404
$^{207}Pb/^{235}$ U	0.51087	0.69716	0.69109	0.71892	0.60723	0.73827	0.56814	0.71849
Error (%)	1.8870	1.8867	1.9305	1.8482	1.9539	1.8526	1.9034	1.9906
$^{206}Pb/^{238}$ U	0.06327	0.08756	0.08533	0.08947	0.07566	0.09152	0.07055	0.08906
Error (%)	1.8521	1.8500	1.9167	1.8104	1.9351	1.8216	1.8531	1.7832
$^{206}Pb/^{238}$ U age (million years)	395	541	528	552	470	565	439	550
$^{207}Pb/^{235}$ U age (million years)	419	537	533	550	482	561	457	550
$^{207}Pb/^{206}$ U age (million years)	551	520	557	540	538	549	545	549

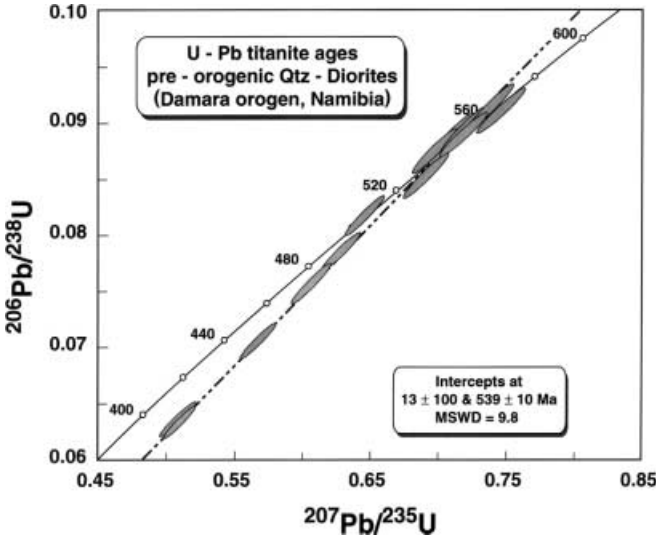

Fig. 2. U/Pb concordia diagram showing titanite analyses from quartz diorites

with decreasing ϵ_{Nd} values and increasing initial $^{87}Sr/^{86}Sr$ values.

Generally, all quartz diorite samples show rather low $\delta^{18}O$ values (Table 5). The variation of $\delta^{18}O$ for quartz diorites from Goas is between 7.5 and 8.1‰ and between 6.8 and 7.8‰ for samples from Okongava. Most of these values are lower than those reported for other Damaran quartz diorites (7.8–9.9‰; Haack et al. 1982) and other granitoids from the Damara belt (Haack et al. 1982; Jung et al. 1998b, 1999, 2001). Generally, they are more typical of mafic crustal rocks than of mafic rocks that contain a mantle component.

Discussion

The quartz diorites from Goas and Okongava are among the least evolved granitoids of the Damara orogen with low SiO_2, relatively high MgO and low Sr isotope compositions. Geochemical features diagnostic for primary mafic magmas (e.g. Ni > 300 ppm, Cr: > 500 ppm) are not applicable for the quartz diorites because the variation in Nd, Pb and O isotope composition precludes a derivation of the quartz diorites from common upper mantle sources. In principle there are three main possibilities for the derivation of the primitive quartz diorite magmas: (1) melting of upper mantle previously enriched by subduction, (2) melting of less enriched or even depleted mantle followed by crustal contamination and (3) melting of mafic lower crust. However, Sr, Nd, Pb and O isotope compositions are heterogeneous, thus precluding a simple closed-system partial melting/fractionation model for the origin of the quartz diorite suites. Therefore, in order to constrain the partial melting process and possible sources of the quartz diorites, it is necessary to evaluate simple fractionation processes with and without assimilation of crustal material.

Fractional crystallization processes

Both suites of quartz diorites are distinct, but a general fractional crystallization trend is indicated by decreasing TiO_2, MgO, FeO, CaO, Al_2O_3, P_2O_5, V, Cr, Ni, Y, Zr, Sr, Ba concentrations and U/Pb ratios and increasing K_2O, Rb and Th concentrations, and Th/U ratios with increasing SiO_2 (Figs. 3 and 4). These trends can be interpreted to indicate fractionation of amphibole, Fe–Ti-oxides, plagioclase and minor amounts of apatite. Figure 8 is an evaluation of the most likely fractionating mineral assemblage in terms of Rb and Sr concentrations. The smooth negative correlation between Rb and Sr can be explained by fractionation of 30% amphibole and 70% plagioclase. In the quartz diorites, the negative Eu anomaly (expressed as Eu/Eu*) increases with decreasing Sr (Fig. 9) and Ga concentrations, indicating that plagioclase plays a major role during fractional crystallization. There is also a positive correlation of Ga

Table 3. Major (in wt%) and trace element (in ppm) composition of quartz diorites from the Damara orogen (Namibia). *LOI* Loss on ignition; *FeO** all Fe as Fe^{2+}; *ASI* alumina saturation index; *X Mg* MgO/(MgO + FeO*); *Eu/Eu** europium anomaly; *n.d.* not determined

Location of sample	Goas								
	M20	M21	M22	M24	M25	M26	M27	M29	M30
SiO_2	58.56	57.96	56.32	61.17	58.76	61.75	58.65	57.93	56.93
TiO_2	0.92	0.93	1.18	0.73	0.92	0.77	0.92	0.92	1.08
Al_2O_3	17.34	17.60	17.64	16.86	17.48	16.98	17.50	17.42	16.99
Fe_2O_3	1.89	2.44	2.76	1.38	2.28	2.08	2.52	2.29	2.34
FeO	5.08	4.64	5.50	4.44	4.73	3.60	4.29	4.78	5.78
MnO	0.14	0.14	0.20	0.13	0.14	0.13	0.16	0.16	0.19
MgO	2.74	2.83	3.37	2.36	2.88	2.33	2.68	3.01	3.60
CaO	6.15	6.24	6.75	5.31	5.99	5.44	5.64	6.49	6.72
Na_2O	2.68	2.78	3.06	2.64	2.66	2.79	2.85	2.62	2.39
K_2O	2.13	2.25	2.42	2.47	2.52	2.69	2.93	2.36	2.19
P_2O_5	0.23	0.24	0.32	0.20	0.24	0.20	0.27	0.22	0.28
LOI	1.25	1.08	0.83	0.77	0.83	0.72	0.77	1.22	0.80
Total	99.11	99.13	100.35	98.46	99.43	99.48	99.18	99.42	99.29
Sc	13	19	20	14	14	13	16	17	20
V	113	126	136	95	116	89	115	128	163
Cr	n.d.	n.d.	36	n.d.	44	32	39	30	43
Co	4	31	18	25	8	11	32	20	9
Ni	n.d.	n.d.	22	n.d.	18	18	21	20	27
Zn	83	83	114	71	90	76	94	86	97
Ga	20	20	22	14	19	22	24	23	19
Rb	86	94	101	99	99	100	112	92	88
Sr	517	531	506	472	503	488	487	554	511
Y	21	23	32	16	23	18	24	24	25
Zr	228	223	271	190	214	180	253	186	242
Nb	12	15	19	14	11	19	20	10	16
Ba	811	848	889	733	886	791	939	784	906
Pb	24	25	29	26	22	25	27	25	27
Th	9	11	8	12	10	15	13	11	9
U	3	3	3	2	3	2	3	4	2
Fe^{2+}/Fe^{3+}	0.37	0.53	0.50	0.31	0.48	0.58	0.59	0.48	0.40
FeO*	6.78	6.83	7.98	5.68	6.78	5.47	6.56	6.84	7.88
ASI	0.97	0.96	0.88	1.01	0.97	0.98	0.97	0.93	0.92
Na_2O/K_2O	1.26	1.24	1.26	1.07	1.06	1.04	0.97	1.11	1.09
*X*Mg	0.85	0.82	0.83	0.87	0.83	0.82	0.81	0.84	0.86
Rb/Sr	0.17	0.18	0.20	0.21	0.20	0.20	0.23	0.17	0.17
Rb/Ba	0.11	0.11	0.11	0.14	0.11	0.13	0.12	0.12	0.10
Sr/Ba	0.64	0.63	0.57	0.64	0.57	0.62	0.52	0.71	0.56
La	50.9	46.2	40.0	43.9	45.7	50.2	55.6	39.9	57.1
Ce	97.0	92.6	82.9	93.1	91.5	99.6	111.1	85.1	119.0
Nd	34.6	36.6	36.5	31.2	34.8	36.7	39.0	33.8	50.5
Sm	6.51	7.48	7.43	4.86	5.54	7.07	6.78	6.20	8.19
Eu	1.74	2.34	2.27	1.04	1.30	1.58	1.67	1.76	2.68
Gd	4.92	7.74	7.20	4.19	4.83	5.22	4.17	4.92	8.34
Dy	4.73	6.00	7.21	3.58	3.91	4.05	3.52	4.63	6.45
Er	2.80	3.00	3.48	2.18	2.20	2.20	2.00	2.76	3.19
Yb	2.20	2.40	2.78	2.03	2.10	2.00	1.78	2.30	2.61
Lu	0.31	0.34	0.37	0.30	0.30	0.30	0.24	0.35	0.40
Eu/Eu*	0.96	0.88	0.91	0.67	0.74	0.82	1.03	0.97	0.94

concentrations with the size of the negative Eu anomaly; samples with low Ga concentrations display the strongest Eu anomaly. Fractionation between LREE and HREE can also monitor fractional crystallization processes. The Ce/Yb_N ratio increases and the Yb_N concentration decreases with decreasing TiO_2 (Fig. 10), suggesting modification of the Ce/Yb_N ratio and the Yb concentration during fractional crystallization. Enrichment of LREE, together with depletion of HREE during fractional crystallization, are compatible with fractionation of amphibole, which tends to concentrate the HREE.

Contamination

From Fig. 11, it is evident that the Sr, Nd, Pb and O isotope composition show a systematic behaviour with respect to major element chemistry. Initial $^{87}Sr/^{86}Sr$ and $\delta^{18}O$ values increase whereas initial ϵ_{Nd}, $^{207}Pb/^{204}Pb$ and $^{208}Pb/^{204}Pb$ decrease with decreasing MgO concentration (Fig. 11). These features indicate that during crystal fractionation processes (i.e. decreasing MgO), assimilation of country rock material substantially modified the isotopic composition. There is also a positive correlation between $\delta^{18}O$ and initial $^{87}Sr/^{86}Sr$ and between ϵ_{Nd} and

Table 4. Major (in wt%) and trace element (in ppm) composition of quartz diorites from the Damara orogen (Namibia). *LOI* Loss on ignition; *FeO** all Fe as Fe^{2+}; *ASI* alumina saturation index; *XMg* MgO/(MgO + FeO*); *Eu/Eu** europium anomaly; *n.d.* not determined

Location of sample	Okongawa									
	M31	M33	M34	M35	M37	M38	M39	M40	M41	M42
SiO_2	55.59	57.58	59.47	58.94	57.58	57.76	55.81	55.66	57.58	51.57
TiO_2	1.17	1.08	0.87	1.04	0.97	0.99	1.07	1.08	1.12	1.29
Al_2O_3	17.77	15.05	15.78	15.02	16.62	15.84	16.52	17.22	17.04	17.53
Fe_2O_3	2.32	2.58	1.91	2.41	2.41	2.37	2.13	2.72	2.97	3.72
FeO	5.71	5.13	4.42	5.27	4.61	4.84	5.69	5.32	4.51	5.78
MnO	0.17	0.18	0.13	0.17	0.14	0.14	0.15	0.14	0.14	0.18
MgO	3.13	4.04	2.84	3.52	3.37	3.69	3.78	2.98	2.95	4.66
CaO	6.40	6.64	5.42	5.80	6.14	6.19	6.88	6.47	6.15	8.35
Na_2O	2.93	2.39	2.89	2.38	2.73	2.71	2.70	2.91	2.91	2.78
K_2O	2.67	2.86	3.12	2.95	3.17	2.55	2.42	2.26	2.69	1.70
P_2O_5	0.34	0.23	0.20	0.26	0.24	0.25	0.25	0.27	0.26	0.30
LOI	0.95	0.89	2.25	1.07	0.91	1.25	1.06	1.22	0.47	0.75
Total	99.15	98.65	99.30	98.83	98.89	98.58	98.46	98.25	98.79	98.61
Sc	11	28	18	25	26	18	23	20	19	23
V	119	176	137	164	150	161	180	171	155	227
Cr	65	50	n.d.	52	62	n.d.	n.d.	n.d.	41	76
Co	4	46	35	20	22	32	43	41	16	40
Ni	35	33	n.d.	32	26	n.d.	n.d.	n.d.	21	38
Zn	116	91	71	97	86	83	90	89	87	105
Ga	23	16	18	19	22	21	17	18	21	22
Rb	100	97	118	130	117	102	91	78	94	60
Sr	489	437	447	372	494	534	485	496	480	578
Y	22	29	21	27	26	25	23	22	20	33
Zr	245	195	189	221	182	208	222	235	241	280
Nb	16	18	15	18	14	14	15	14	14	14
Ba	850	856	789	789	930	711	731	764	916	708
Pb	29	28	30	31	31	31	23	28	34	23
Th	10	16	21	17	12	16	13	10	14	10
U	3	2	2	3	2	2	3	2	3	2
Fe^{2+}/Fe^{3+}	0.41	0.50	0.43	0.46	0.52	0.49	0.37	0.51	0.66	0.64
FeO*	7.80	7.45	6.14	7.44	6.78	6.97	7.60	7.77	7.18	9.12
ASI	0.92	0.79	0.88	0.85	0.87	0.86	0.84	0.91	0.90	0.81
Na_2O/K_2O	1.10	0.84	0.93	0.81	0.86	1.06	1.12	1.29	1.08	1.64
*X*Mg	0.84	0.86	0.85	0.85	0.85	0.86	0.88	0.81	0.80	0.83
Rb/Sr	0.20	0.22	0.26	0.35	0.24	0.19	0.19	0.16	0.20	0.10
Rb/Ba	0.12	0.11	0.15	0.16	0.13	0.14	0.12	0.10	0.10	0.08
Sr/Ba	0.58	0.51	0.57	0.47	0.53	0.75	0.66	0.65	0.52	0.82
La	68.8	42.6	43.7	50.5	29.5	34.6	35.3	40.7	48.1	35.6
Ce	119.5	89.2	84.3	102.3	69.8	70.9	73.7	84.9	97.3	73.2
Nd	41.8	39.5	33.3	45.4	30.8	32.4	33.2	33.7	36.6	33.6
Sm	8.09	9.32	6.05	8.23	6.66	6.47	6.74	6.40	7.78	6.70
Eu	1.99	1.88	1.43	1.36	1.13	1.43	1.38	1.49	1.91	1.86
Gd	5.56	7.56	5.52	6.27	4.92	5.63	5.15	5.43	6.41	6.07
Dy	4.55	5.86	3.54	4.48	4.24	4.31	4.78	4.31	4.84	5.04
Er	2.38	2.93	1.80	2.10	2.04	2.20	2.50	2.10	2.50	2.50
Yb	2.50	2.44	1.50	2.00	1.68	1.60	2.00	1.80	2.00	2.40
Lu	0.40	0.37	0.25	0.36	0.24	0.25	0.26	0.25	0.31	0.35
Eu/Eu*	0.97	0.71	0.72	0.60	0.62	0.71	0.73	0.76	0.84	0.86

$^{207}Pb/^{204}Pb$, and a negative correlation between $\delta^{18}O$ and $^{207}Pb/^{204}Pb$ and ϵ_{Nd} and also between $^{87}Sr/^{86}Sr$ and ϵ_{Nd}, which further indicate contamination processes.

The composition of the quartz diorites and two different Damara country rocks (Jung et al. unpublished) are shown in a diagram of $^{87}Sr/^{86}Sr$ vs Sr concentration (Fig. 12). The country rocks are a typical Damara metapelite ($^{87}Sr/^{86}Sr$: 0.720, Sr: 200 ppm) and an evolved basement gneiss of inferred Proterozoic to Archaean age ($^{87}Sr/^{86}Sr$: 0.740, Sr: 500 ppm) because it can be expected that such lithologies are the most fusible parts of a crustal segment and, thus, are most likely involved in any assimilation scenario. The most mafic quartz diorite with ca. 50 wt% SiO_2 has ca. 600 ppm Sr, a primitive Sr isotopic composition and only a small negative Eu-anomaly; therefore, it is considered to represent one of the least contaminated end members. The most likely AFC curves to fit the data are those of the metapelitic end member with 200 ppm Sr and $^{87}Sr/^{86}Sr$: 0.7200 (case A) and the pre-Damara orthogneiss (case B). Decreasing Al_2O_3, Sr and Ga concentrations and increasing Eu/Eu* shows that plagioclase strongly controls the fractionating assemblage and, therefore, the bulk K_d for Sr has to be >1. The value of r ($r =$ ratio of assimilation to

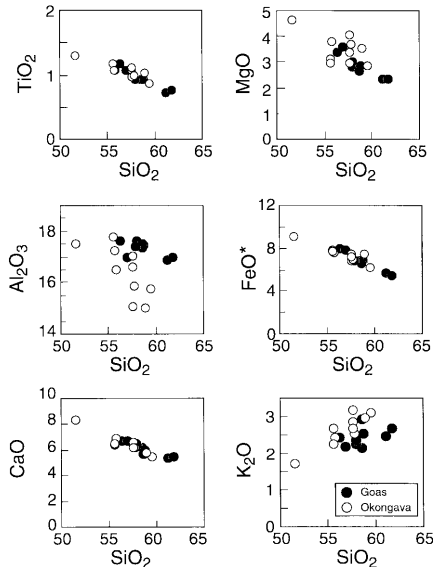

Fig. 3. Major element plots for both types of quartz diorite

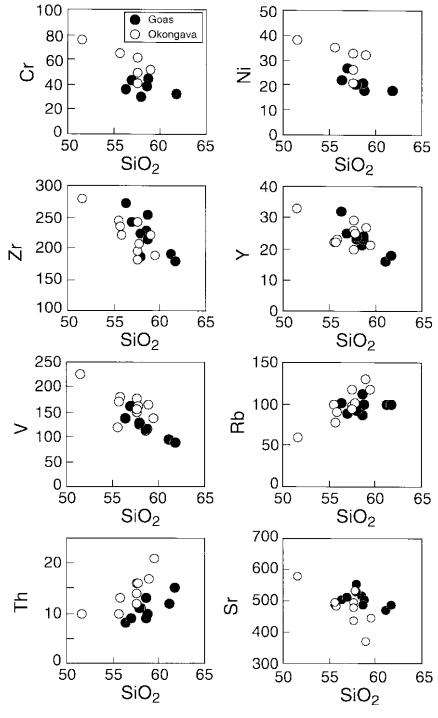

Fig. 4. Selected trace element plots for both types of quartz diorite

fractionation) was set at 0.8 and the amount of assimilation is estimated to be $< 10\%$, suggesting that only a small fraction of crustal material was assimilated. In contrast to previous estimates for the ratio of mass assimilated to mass fractionated (r: $< < 1$; DePaolo 1981) higher values of r (r: 1–2; Reiners et al. 1995) may be possible. High values of r further suggest that assimilation took place in the deep crust at high temperatures.

Processes of crustal assimilation can also be illustrated by using different isotope systems. Figure 13

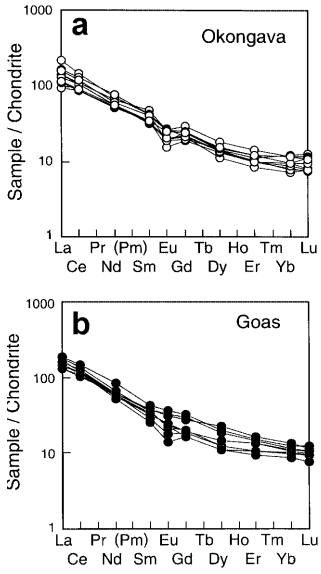

Fig. 5. Chondrite-normalized rare earth element plots for both types of quartz diorite. Normalization factors according to Boynton (1984)

shows that the negative correlation between Sr and Nd and the positive correlation between Sr and O isotope composition is best monitored by using an orthogneiss from the pre-Pan African basement as the contaminant. Lead isotope compositions are not available from basement gneisses; however, the Pb isotope composition is particularly susceptible to extreme changes during AFC as a result of the high concentration of Pb in felsic crustal rocks relative to mafic rocks. Therefore, it is very likely that compositional differences in the contaminant are responsible for changes in Pb isotope composition. Lead isotope composition correlates with Nd and Sr isotope compositions and increasing contamination is accompanied by decreasing ϵ_{Nd}, increasing $^{87}Sr/^{86}Sr$, but decreasing $^{207}Pb/^{204}Pb$ and $^{208}Pb/^{204}Pb$ ratios. This relationship indicates that the source of the contaminant has a lower μ and κ value than the quartz diorites.

Partial melting processes and magma sources

Sill-like intrusions are thought to be a major component of mid- to lower crustal regions (Bohlen 1987) although, in the Damara orogen, geophysical evidence (Green 1983) argue against the existence of large volumes of mafic rocks in the lower crust. However, recent work by Petford and Gallagher (2001) indicates that these sills need not be very thick in order to melt mafic lower crust. Experimental evidence (Helz 1976; Beard and Lofgren 1991; Rapp et al. 1991; Rushmer 1991; Wolf and Wyllie 1994; Rapp and Watson 1995) and theoretical considerations (Roberts and Clemens 1993) suggests that dehydrating basaltic material within the lower crust can produce significant volumes of mafic partial melts, particularly in regions with high heat flow. Depending on

Table 5. Rb–Sr, Sm–Nd, Pb and O isotope data from quartz diorites from the Damara orogen Namibia. *n.d.* Not determined. See Analytical techniques. Uncertainties for the $^{87}Sr/^{86}Sr$ and $^{143}Nd/^{144}Nd$ are 2σ (mean) errors in the last two digits. ϵ Nd values at the time of intrusion (Tables 3 and 4) are calculated relative to CHUR with present-day values of $^{143}Nd/^{144}Nd = 0.512638$ and $^{147}Sm/^{144}Nd = 0.1966$ (Jacobson and Wasserburg 1980). Nd model ages calculated with a depleted mantle reservoir and present-day values of $^{143}Nd/^{144}Nd = 0.513144$ and $^{147}Sm/^{144}Nd = 0.222$ (Michard et al. 1985). *m* Measured; *i* initial

Sample	$^{147}Sm/^{144}Nd$ (m)	$^{143}Nd/^{144}Nd$ (m)	Sm (ppm)	Nd (ppm)	$^{143}Nd/^{144}Nd$ (i)	ϵ Nd (i)	T_{DM} (Ga)	$^{87}Sr/^{86}Sr$ (m)	$^{87}Rb/^{86}Sr$	$^{87}Sr/^{86}Sr$ (i)	Rb (ppm)	Sr (ppm)	$\delta^{18}O$ (‰)	$^{206}Pb/^{204}Pb$	$^{207}Pb/^{204}Pb$	$^{208}Pb/^{204}Pb$
M 20	0.1027	0.51163	6.724	39.56	0.511264 (12)	−13.0	1.9	0.716132 (16)	0.4745	0.712412	87.20	532.1	7.78	17.223	15.556	37.804
M 21	0.1077	0.51162	6.981	39.19	0.511227 (11)	−13.7	2.0	0.716180 (15)	0.4759	0.712449	89.72	545.9	7.65	17.210	15.553	37.901
M 22	0.1234	0.51170	7.349	36.01	0.511256 (10)	−13.2	2.2	0.716704 (14)	0.5675	0.712254	98.91	504.6	7.50	17.230	15.563	37.903
M 24	0.0968	0.51153	4.926	30.74	0.511183 (13)	−14.6	1.9	0.715888 (14)	0.5993	0.711189	100.9	487.2	7.90	17.180	15.535	37.707
M 25	0.1049	0.51156	6.563	37.83	0.511185 (09)	−14.6	2.0	0.716778 (14)	0.5013	0.712848	96.85	503.5	8.00	n.d.	n.d.	n.d.
M 26	0.1066	0.51159	7.303	41.40	0.511207 (09)	−14.1	2.0	0.715792 (14)	0.5814	0.711233	99.84	497.2	8.02	17.185	15.541	37.726
M 27	0.1020	0.51155	6.801	40.30	0.511180 (06)	−14.6	2.0	0.716311 (18)	0.6340	0.711340	108.2	494.0	7.75	17.172	15.556	37.774
M 29	0.1147	0.51164	6.214	32.74	0.511230 (14)	−13.7	2.1	0.715023 (16)	0.4862	0.711211	92.22	549.1	8.14	17.170	15.546	37.853
M 30	0.1093	0.51167	8.362	49.24	0.511274 (08)	−12.8	2.0	0.714599 (12)	0.4836	0.710807	87.54	524.0	7.90	17.157	15.545	37.799
M 31	0.1075	0.51154	8.041	45.22	0.511151 (09)	−15.2	2.1	0.717236 (14)	0.6029	0.712509	100.0	480.2	7.50	17.119	15.576	37.797
M 33	0.1199	0.51825	8.499	42.86	0.511393 (08)	−10.5	1.9	0.716029 (12)	0.6700	0.710776	102.0	439.9	7.73	17.121	15.611	38.156
M 34	0.1082	0.51178	6.137	34.29	0.511391 (06)	−10.5	1.8	0.717386 (12)	0.8072	0.711057	120.3	431.4	7.80	17.126	15.586	38.053
M 35	0.1033	0.51176	9.199	53.84	0.511391 (07)	−10.5	1.7	0.718190 (18)	0.9375	0.710839	126.8	391.6	7.50	17.109	15.572	37.994
M 37	0.1227	0.51182	6.375	31.39	0.511377 (07)	−10.8	2.0	0.716342 (16)	0.6657	0.711123	118.7	516.1	7.20	17.139	15.593	38.107
M 38	0.1111	0.51186	6.281	34.18	0.511462 (08)	−9.1	1.7	0.713470 (13)	0.5154	0.709429	96.29	540.8	7.20	17.161	15.591	38.075
M 39	0.1159	0.51188	6.753	35.22	0.511461 (06)	−9.2	1.8	0.714211 (10)	0.5283	0.710069	88.53	485.1	6.80	17.170	15.625	38.051
M 40	0.1069	0.51162	6.657	36.70	0.511224 (08)	−13.8	2.0	0.715232 (10)	0.4292	0.711867	72.89	491.6	7.45	17.110	15.594	38.051
M 41	0.1105	0.51162	7.147	39.11	0.511217 (06)	−13.9	2.0	0.716474 (13)	0.5470	0.712185	91.17	482.6	7.43	17.083	15.558	37.857
M 42	0.1146	0.51185	6.520	34.38	0.511437 (07)	−9.7	1.8	0.712595 (13)	0.2903	0.710319	61.13	609.5	6.90	17.160	15.615	37.957

Fig. 6. Initial ϵ_{Nd} versus initial $^{87}Sr/^{86}Sr$ diagram for quartz diorites

Fig. 7. Plot of **a** $^{207}Pb/^{204}Pb$ and **b** $^{208}Pb/^{204}Pb$ versus $^{206}Pb/^{204}Pb$ isotope ratios of leached K-feldspar from quartz diorites. The curve represent the average Pb growth curve according to Stacey and Kramers (1975). *Tick marks* represent 250-Ma intervals

Fig. 8. Variation in Rb and Sr concentration within the quartz diorites. *Symbols* as in Fig. 3. Mineral vectors calculated according to partition coefficients compiled in Rollinson (1993). Compositional trend of the quartz diorites indicate fractionation of ca. 30 wt% of plagioclase and ca. 70 wt% of hornblende

bulk composition, dehydration melting of amphibolite yields 10–60% quartz diorite to tonalite melt at temperatures of 900–1,000 °C, whereas H_2O-saturated melting yields similar amounts of granite melt at lower temperatures of between 850 and 900 °C.

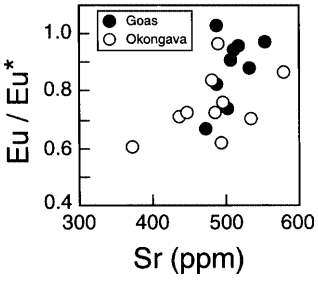

Fig. 9. Plot of Eu/Eu* as a measure of the negative Eu anomaly vs. Sr concentrations for both suites of quartz diorites. For discussion see text

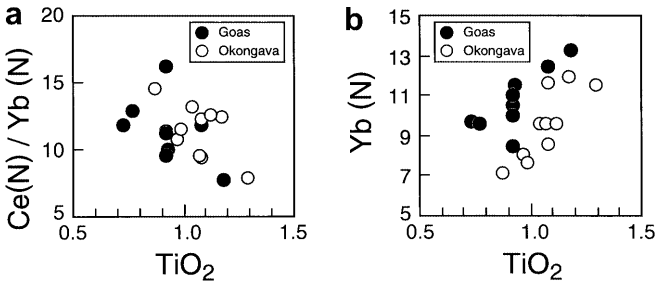

Fig. 10. Plot of **a** Ce/Yb_N and **b** Yb_N vs TiO_2. Correlation between the parameters indicate strong influence of crystal fractionation processes upon REE systematics

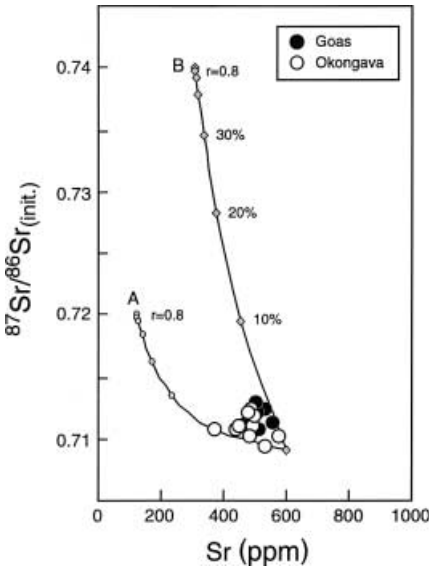

Fig. 12. Plot of $^{87}Sr/^{86}Sr$ vs. Sr concentration for quartz diorites and calculated AFC curves using two hypothetical country rocks (*A* pelite with 200 ppm Sr and $^{87}Sr/^{86}Sr$: 0.7250, and *B* meta-igneous basement gneiss with 500 ppm Sr and $^{87}Sr/^{86}Sr$: 0.7400). Bulk K_D (Sr) was 1.5. The hypothetical source rock contains 600 ppm Sr and $^{87}Sr/^{86}Sr$: 0.7090 similar to the most primitive quartz diorite sample M42

Some of the quartz diorites have chemical features that are characteristic of partial melts derived from metabasaltic rocks. They have low SiO_2, high Al_2O_3, moderately high Na_2O/K_2O, high LREE concentrations, moderately low HREE concentrations and the most primitive rocks do not display a negative Eu anomaly. Based on previous work (Rapp et al. 1991; Wolf and Wyllie 1993; Rapp and Watson 1995), the highest pressure partial melts should have the lowest Y and HREE concentrations, but the highest Al_2O_3 and Sr concentrations and the highest Sr/Y ratios. For the quartz diorites from the Damara orogen, those with the lowest Y concentration and highest Sr/Y have the highest Al_2O_3 and least negative Eu anomaly. All these characteristics would be expected for partial melts from a basaltic protolith, most probably a garnet-bearing amphibolite at high pressures. An amphibole-bearing residue for the quartz diorites of the Damara orogen is consistent with the low TiO_2 concentrations and low Rb/Sr and K/Rb ratios, despite their high absolute K and Rb concentrations (Petford and Atherton 1996).

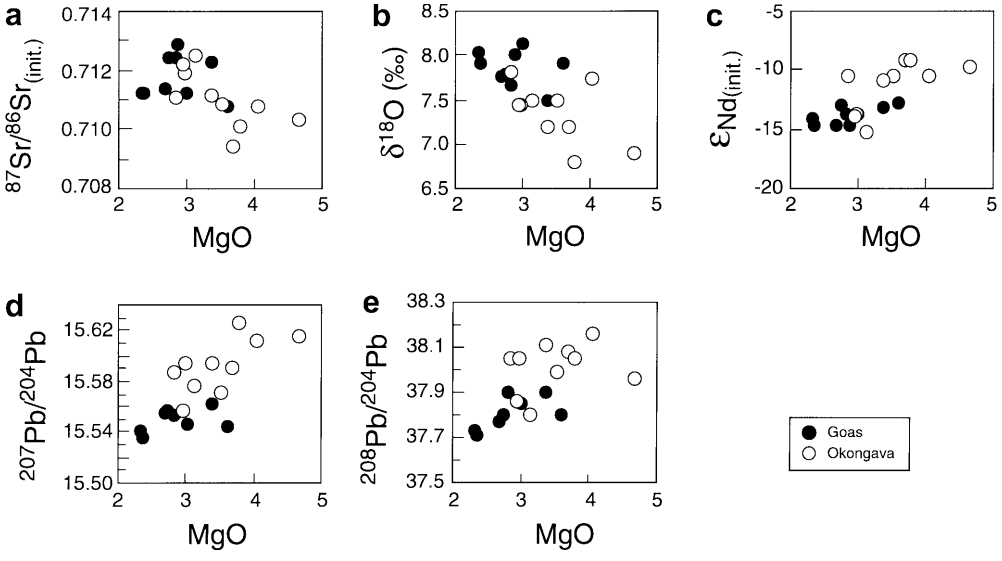

Fig. 11. Variation of $^{87}Sr/^{86}Sr$, $\delta^{18}O$, ϵ Nd, $^{207}Pb/^{204}Pb$, $^{208}Pb/^{204}Pb$ vs. MgO. The trends are best explained by assimilation of evolved country rocks during fractional crystallization. Note that the contaminant must be more evolved in Sr, Nd and O isotope composition, but must have lower μ and κ values

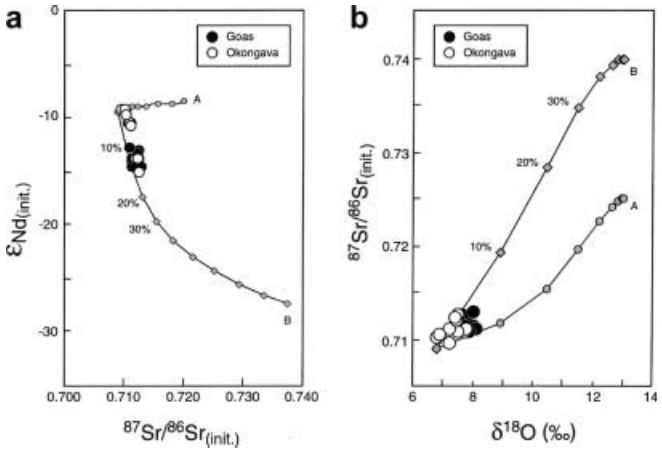

Fig. 13. Plot of **a** $^{87}Sr/^{86}Sr$ vs. ϵ_{Nd} and **b** $^{87}Sr/^{86}Sr$ vs. $\delta^{18}O$ for quartz diorites and calculated AFC curves using the same two hypothetical country rocks as in Fig. 12. *A* pelite with 200 ppm Sr $^{87}Sr/^{86}Sr$: 0.7250, ϵ_{Nd}: –8.4, $\delta^{18}O$: 13‰ and *B* meta-igneous basement gneiss with 500 ppm Sr, $^{87}Sr/^{86}Sr$: 0.7400, ϵ_{Nd}: –29, $\delta^{18}O$: 13‰. Bulk K_D (Sr) was 1.5 and bulk K_D (Nd) was 0.8. A *r*-value (ratio of assimilation to fractionation) of 0.8 was used. The hypothetical source rock has 600 ppm Sr, $^{87}Sr/^{86}Sr$: 0.7090, ϵ_{Nd}: –9.4, $\delta^{18}O$: 6.8‰ similar to quartz diorite sample M42

The quartz diorites from the Damara orogen have $K_2O > 2.5$ wt%, MgO > 3 wt%, CaO > 6 wt%, FeO_{total} > 7 wt% and TiO_2 > 1.0 wt%. Such chemical characteristics are observed only in experiments performed between 1,000–1,100 °C at high pressures (Fig. 14). Abundances of MgO are similar in the quartz diorites and in the experimental melts derived by melting of low

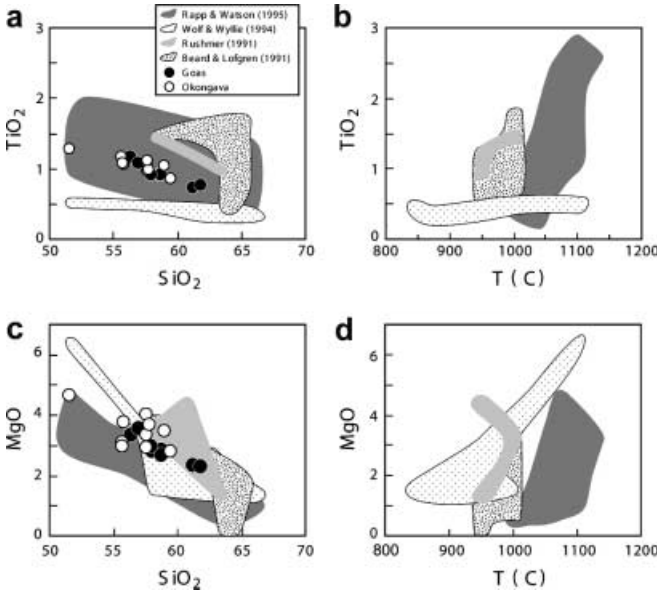

Fig. 14. Plot of **a** TiO_2 and **b** MgO vs. SiO_2, **c** TiO_2 and **d** MgO vs. temperature for quartz diorites and experimental investigations. Note that the composition of the quartz diorites is likely reproduced by high-temperature melting of a source similar to the low-K (medium-K?) ol-tholeiite of Rapp and Watson (1995). For further discussion see text

K-basaltic rocks (Wolf and Wyllie 1994; Rapp and Watson 1995), but substantially higher than in melts generated by melting of alkali basaltic and high-Al basaltic sources. Similarly, the high CaO concentrations in the quartz diorites precludes alkali basaltic sources and the low TiO_2 abundances suggests that high-Al basaltic sources are also unlikely sources. Overall, the source rock of the quartz tholeiites is most likely a high-grade metamorphic, medium-K basaltic rock that melted at high temperatures and high pressures in the lower crust.

At 10–15 kbar, calc-alkaline liquids coexist with garnet under both vapour-saturated and undersaturated conditions (Huang and Wyllie 1986; Rutter and Wyllie 1988; Carrol and Wyllie 1990). None of the most primitive quartz diorites show the significant HREE depletion (i.e. $Yb_N < 10$; Wareham et al. 1997) predicted for melts that equilibrated with residual garnet, suggesting that they formed alternatively under lower pressures, with less garnet in the residuum or that garnet was melted to a large extent during formation of the melts. However, the high temperatures required for amphibolite melting restrict this process to the deep crust. Temperatures in the deep crust during generation of the quartz diorites cannot have exceeded 1,070 °C at 10–15 kbar, which is the thermal stability limit of amphibole in basalt (Allen and Boettcher 1978). Comparison with experimental results (Fig. 14) support the idea of high-temperature generation of the quartz diorites because the major element concentrations are only reproduced in high-temperature runs between 1,000–1,100 °C. The temperature at which a mafic melt separated from its source may be estimated from its P_2O_5 concentration, using the apatite solubility expression of Harrison and Watson (1984). This approach assumes that the melt formed in equilibrium with residual apatite and has not undergone subsequent modification by processes related to fractional crystallization or assimilation. The first requirement may be satisfied during melting, especially at low degrees of melting, but the second requirement is more difficult to evaluate. However, the most mafic quartz diorites have the most primitive isotopic composition indicating less modification by AFC processes. For these samples P_2O_5 concentrations are between 0.32–0.34 wt%, indicating temperatures of between 1,060 and 1,070 °C, similar to those given by the experimental investigations.

Summary and discussion of model

Miller (1983) and Kasch (1983) used the occurrence of quartz diorites as an argument for an island arc setting of the southern part of the Central Zone of the Damara orogen. Despite the striking absence of geological evidence for a subduction zone setting, it is pertinent to compare the chemistry of the quartz diorites with that of magmatic rocks from arc environments. The low concentrations of Ni and Cr argue against a pure mantle derivation of the quartz diorites; however, similar low

abundances have been reported in the least evolved members of some island arc tholeiite and calc-alkaline series (e.g. Perfit et al. 1980). A number of trace element characteristics are typical for arc magmatism, i.e. enrichment of LILE (Ba, Rb, K), relative depletion of HFSE (e.g. Nb) and, consequently, high LILE/HFSE ratios. Enrichment of LILE might be caused by transfer of volatiles from dehydrating subducted oceanic crust to the mantle wedge (e.g. Hawkesworth et al. 1979a, 1979b; Thirlwall and Graham 1984, among many others). In the absence of a subduction zone setting, enrichment of LILE may be caused by preferential tapping of enriched mantle sources (e.g. Saunders et al. 1980) or may be caused by AFC (assimilation-fractional crystallization) or MASH (melting–assimilation–storage–homogenization) processes (e.g. Hildreth and Moorbath 1988). Despite the striking evidence for AFC processes, the least evolved quartz diorite samples have rather low SiO_2 contents, but unradiogenic Nd and radiogenic Sr isotope composition. While large-scale crustal contamination of magma derived from upper mantle sources could explain some of the isotope variation, such contamination would likely be accompanied by strong fractional crystallization, which is not observed. Furthermore, the strongly retarded Pb isotope compositions precludes their derivation from a common or even moderately enriched upper mantle source at 550 Ma. The Sr–Nd isotope composition of the quartz diorites is unlike the Sr–Nd isotope composition of other Damara granites for which a upper crustal derivation (McDermott et al. 1996; Jung et al. 2001), a lower crustal derivation (Jung et al. 2002) or even a contribution from the lithospheric mantle (Jung et al. 1998b) has been inferred. It is also unlike the Nd and Sr isotope composition of other quartz diorites from the Damara orogen. Although similar in age (ca. 550 Ma), these rocks are situated farther north and have different isotope compositions ($^{87}Sr/^{86}Sr$: 0.7045–0.7053; ϵ_{Nd}: –0.1; $\delta^{18}O$: 7.8–9.1‰, Hawkesworth et al. 1981; Haack et al. 1982). Therefore, it is very likely that the isotope composition of the quartz diorites studied here matches the composition of the mafic lower crust beneath the Damara orogen.

Previous studies have shown that Pb isotopes from leached feldspars provide useful information for the understanding of crustal evolution and often record evidence for an ancient crustal memory. Magmatic differentiation and metamorphic events can produce significant variations in μ and κ values, which lead to highly variable Pb isotope ratios. Lead isotope ratios from leached feldspars are useful, because feldspars have low μ and κ values and their Pb isotope compositions can be used to estimate the initial Pb isotope ratios at the time of the last equilibration event. The quartz diorites have the most retarded Pb isotope compositions so far recorded in Damaran plutonic rocks. The samples plot well above the Stacey and Kramers (1975) Pb evolution curve at a Pb model age of ca. 1 Ga. Although strongly retarded, these isotopic features suggest that the diorites cannot come from a MORB-type source. The large variation in $^{207}Pb/^{204}Pb$ relative to $^{206}Pb/^{204}Pb$ indicate the involvement of old reworked crust and is probably also a result of the influence of an ancient sedimentary component. High-grade metamorphism during ancient events in deep crustal sources can lead to strongly retarded Pb isotope compositions because of fractionation of U from Pb and Th from U. Although both elements, U and Th, are highly incompatible, U is more soluble than Th and is preferentially incorporated into a fluid phase whereas Th is practically insoluble in a fluid phase, but strongly partitioned into a melt (e.g. Taylor and McLennan 1985). Therefore, it is very likely that the observed Pb isotope composition is the result of both high-grade metamorphism and melting. Considering the retarded composition these depletion events must be significantly older than 550 Ma.

The most plausible model for the generation of the quartz diorites that accounts for the observed geochemical features involves partial melting of pre-Pan African mafic lower crust probably because of underplating of mantle-derived magmas. Melting of this lower crust would be most efficient if the partial melting event immediately followed the underplating event and probably close to the onset of high-grade metamorphism because high temperatures are required for such melting events (Petford and Gallagher 2001). It is important to note that the oldest Sm–Nd whole rock garnet ages and U–Pb monazite ages are ca. 540 Ma for the central part of the Damara orogen (Jung and Mezger 2000; Jung et al. 2000b; Jung and Mezger 2002). Therefore, it is reasonable to assume that the crust was already hot at 540 Ma, but it is also very likely that similar quartz diorites are a precursor to high-grade metamorphism, melting and granite formation. Intrusion of large volumes of basaltic rocks are not reported from the Damara orogen, but close to the occurrence of the quartz diorites and a number of independent syenites, some of them ne-normative, intruded the area close to a major shear zone. This shear zone, or parts of it, might have promoted the ascent of mantle-derived syenites, but also lower crustal melts at a time when most of the orogen underwent compression because of thickening and thrusting. New high precision U–Pb titanite ages seem to indicate that the syenites intruded between 590 and 490 Ma; however, the majority of the samples record ages between 520 and 540 Ma (Jung et al. 1998a; unpublished data). This observation outlines a thermal role for mantle-derived magmas in the production of lower crustal melts, but also implies that thick and hot crust is a requirement for the generation of quartz diorites from lower crustal sources. In this model, the crust acts as a barrier to magmas ascending from the mantle, causing them to pond and crystallize, and leading to the development of a zone of lower crustal melting. The overlying crust must have been thick, probably because of thickening during the early stages of orogeny because the quartz diorites evolved by AFC rather than pure FC processes. During intrusion, the quartz diorites assimilated crustal material, which was more radiogenic in

terms of the Sr isotope composition, but less radiogenic in terms of Nd and Pb isotope composition (Fig. 6). These Sr and Nd isotope features are so far only monitored by pre-Pan African basement gneisses as inferred from the isotope composition of basement-derived granites (Jung et al. 2002). The correlation between Sr, Nd, Pb and O isotopes and MgO concentration suggests that during evolution of the quartz diorites more and more evolved (older?) rocks contributed to the isotopic signature of the melts. This behaviour is the opposite of what is expected if an igneous body moves from the site of melting through a crust with the oldest, most evolved rocks underlying the site of melt generation. Therefore, it is reasonable to assume that the area consists of an inverted stratigraphy at depth, in which crustal slices of pre-Pan African basement are intercalated with Pan African rocks. A similar scenario has been suggested for other basement-derived granites elsewhere in the Damara orogen (Jung et al. 2002).

Concluding remarks

Quartz diorites from Okongava and Goas (Damara orogen, Namibia) are the most mafic, but SiO_2-saturated rocks so far discovered in the orogen. Based on temperature estimates based on P_2O_5 solubility in mafic rocks and comparison with results from amphibolite-dehydration melting experiments, melting of a medium-K garnet-bearing metatholeiite at temperatures of between 1,000 and 1,100 °C is likely. The major- and trace element variation is best explained by crystal fractionation processes involving mainly plagioclase (ca. 70%) and hornblende (ca. 30%). Isotope variation suggests that the quartz diorites were modified by AFC processes. Increasing initial Sr isotope ratios, but decreasing Nd isotope ratios, indicate that the contaminant is probably a felsic meta-igneous basement gneiss. The model calculations of AFC require moderately high K_dSr (>1), but low K_dNd (<1), which is supported by the inferred fractionated mineral assemblage of plagioclase and hornblende. However, during AFC processes $^{207}Pb/^{204}Pb$ and $^{208}Pb/^{204}Pb$ ratios decrease with increasing degree of assimilation, suggesting that the source of the contaminant has lower μ and κ values. A high ratio of mass assimilated to mass fractionated further supports lower crustal AFC processes at high temperatures. Although the lower Paleozoic was a time during which a large amount of igneous material was introduced into the upper crust of the Damara orogen it was not a major crust-forming period because most granites studied so far, and also the most mafic rocks such as the quartz diorites studied here, are dominated by recycled crustal material.

Acknowledgements The analytical work was supported by grants from the Max-Planck Society and A.W. Hofmann is thanked for hospitality and free access to mass spectrometry facilities while S.J. held a post-doc position in Mainz. The geochronological work was partly supported under DFG grant Ju 326/1-1 and 326/1-2 to the senior author. E. Hoffer (Marburg) is thanked for free access to ICP facilities and to samples originally collected between 1977–1981 by members of SFB 48 at the University of Göttingen. Iris Bambach (Max-Planck-Institut, Mainz) did a superb job with the line drawings. Special thanks go to D. Dohle and A. Meier from the Bonn fluorine-lab crew for high-precision analyses of oxygen isotopes, to S. Göbeler for determination of REE and to A. Busch and M. Ohnesorge for assistance with the isotope measurements during their stay in Mainz. Finally, we thank Nick Petford and Frank McDermott for constructive reviews.

References

Allen JC, Boettcher AL (1978) Amphiboles in andesite and basalt, II: stability as a function of P–T–f_{H2O}–f_{O2}. Am Mineral 63:1074–1087

Beard JS, Lofgren GE (1991) Dehydration melting and water saturated melting of basaltic and andesitic greenstones and amphibolites at 1, 3 and 6.9 kbar. J Petrol 32:365–402

Bohlen SR (1987) Pressure–temperature–time paths and a tectonic model for the evolution of granulites. J Geol 95: 617–632

Boynton WV (1984) Geochemistry of rare earth elements: meteorite studies. In: Henderson P (ed) Rare earth element geochemistry. Elsevier, Amsterdam, pp 63–114

Briqueu L, Lancelot JR, Valois JP, Walgenwitz F (1980) Géochronologie U–Pb et genèse d'un type de minéralisation uranifère: Les alaskites de Goanikontes (Namibie) et leur encaissant. Bull Cent Rech Elf Aquitaine 4:759–811

Cameron AE, Smith DH, Walker RL (1969) Mass spectrometry of nanogram-size samples of lead. Anal Chem 41:525–526

Carrol MR, Wyllie PJ (1990) The system tonalite–H_2O at 15 kbar and the genesis of cal-alkaline magmas. Am Mineral 75:345–357

Cherniak DJ (1993) Lead diffusion in titanite and preliminary results on the effects of radiation damage on Pb transport. Chem Geol 110:177–194

Clayton RN, Mayeda TD (1963) The use of bromine pentaflouride in the extraction of oxygen from oxides and silicates for isotope analysis. Geochim Cosmochim Acta 27:43–52

DePaolo DJ (1981) A neodymium and strontium isotopic study of the Mesozoic calc-alkaline granitic batholiths of the Sierra Nevada and Peninsular Ranges, California. J Geophys Res 86:10470–10488

Eggins S, Hensen BJ (1987) Evolution of mantle-derived, augite–hypersthene granodiorites by crystal–liquid fractionation: Barrington Tops batholith, eastern Australia. Lithos 20:295–310

Green RWE (1983) Seismic refraction observations in the Damara orogen and flanking craton and their bearing on deep seated processes in the orogen. Spec Publ Geol Soc S Afr 11:355–367

Gromet LP, Silver LT (1987) REE variations across the Peninsular Ranges batholith: implications for batholithic petrogenesis and crustal growth in magmatic arcs. J Petrol 28:75–125

Haack U, Hoefs J, Gohn E (1982) Constraints on the origin of Damaran granites by Rb/Sr and $\delta^{18}O$ data. Contrib Mineral Petrol 79:279–289

Harrison TM, Watson EB (1984) The behaviour of apatite during crustal anatexis: equilibrium and kinetic considerations. Geochim Cosmochim Acta 48:1467–1477

Hartmann O, Hoffer E, Haack U (1983) Regional metamorphism in the Damara orogen: interaction of crustal motion and heat transfer. Spec Publ Geol Soc S Afr 11:233–241

Hawkesworth CJ, Marlow AG (1983) Isotope evolution of the Damara orogenic belt. Spec Publ Geol Soc S Afr 11:397–407

Hawkesworth CJ, O'Nions RK, Arculus RJ (1979a) Nd and Sr isotope geochemistry of island arc volcanics, Grenada, lesser Antilles. Earth Planet Sci Lett 45:237–248

Hawkesworth CJ, Norry MJ, Roddick JC, Baker PE, Francis PW, Thorpe RS (1979b) $^{143}Nd/^{144}Nd$, $^{87}Sr/^{86}Sr$, and incompatible

element variations in calc-alkaline andesites and plateau lavas from South America. Earth Planet Sci Lett 42:45–57
Hawkesworth CJ, Kramers JD, Miller RMG (1981) Old model Nd ages in Namibian Pan-African rocks. Nature 289:278–282
Heaman L, Parrish R (1991) U–Pb geochronology in accessory minerals. In: Heaman L, Ludden J (eds) Short course handbook on application of radiogenic isotope systems to problems in geology, vol 19. Mineralogy Association of Canada, pp 59–102
Heinrichs H, Hermann AG (1990) Praktikum der analytischen Geochemie. Springer, Berlin Heidelberg New York
Helz R (1976) Phase relations of basalt in their melting ranges at P $H_2O = 5$ kb. Part 2. Melt compositions. J Petrol 17:139–193
Hildreth W, Moorbath, S (1988) Crustal contribution to arc magmatism in the Andes of Central Chile. Contrib Mineral Petrol 98:455–489
Hoernes S, Hoffer E (1979) Equilibrium relations of prograde metamorphic mineral assemblages – a stable isotope study of rocks of the Damara orogen. Contrib Mineral Petrol 68:377–389
Huang WL, Wyllie PJ (1986) Phase relationships of gabbro–tonalite–granite–water at 15 kbar with applications to differentiation and anatexis. Am Mineral 71:301–316
Jacobson SB, Wasserburg GJ (1980) Sm–Nd isotope evolution of chondrites. Earth Planet Sci Lett 50:139–155
Jung S, Mezger K (2001) Geochronology in migmatites – a Sm–Nd, U–Pb and Rb–Sr study from the Proterozoic Damara belt (Namibia) and implications for polyphase development of migmatites in high-grade terranes. J Metamorph Geol 19:77–97
Jung S, Mezger K (2002) Petrology of basement-dominated terranes: I. Regional metamorphic T–t path and geochronological constraints on Pan-African high-grade metamorphism (central Damara orogen, Namibia). Chem Geol (submitted)
Jung S, Mezger K, Hoernes S (1998a) Geochemical and isotopic studies of syenites from the Proterozoic Damara belt (Namibia): implications for the origin of syenites. Mineral Mag 62:729–730
Jung S, Mezger K, Hoernes S (1998b) Petrology and geochemistry of post-collisional metaluminous A-type granites – a major and trace element and Nd–Sr–Pb–O-isotope study from the Proterozoic Damara Belt, Namibia. Lithos 45:147–175
Jung S, Mezger K, Masberg P, Hoffer E, Hoernes S (1998c). Petrology of an intrusion-related high-grade migmatite: implications for partial melting of metasedimentary rocks and leucosome-forming processes. J Metamorph Geol 16:425–445
Jung S, Hoernes S, Masberg P, Hoffer E (1999) The petrogenesis of some migmatites and granites (Central Damara Orogen, Namibia): evidence for disequilibrium melting, wall rock contamination and crystal fractionation. J Petrol 40:1241–1269
Jung S, Hoernes S, Mezger K (2000a) Geochronology and petrogenesis of Pan-African syn-tectonic S-type and post-tectonic A-type granite (Namibia) – products of melting of crustal sources, fractional crystallization and wall rock entrainment. Lithos 50:259–287
Jung S, Hoernes S, Mezger K (2000b) Geochronology and petrology of migmatites from the Proterozoic Damara Belt – importance of episodic fluid-present disequilibrium melting and consequences for granite petrology. Lithos 51:153–179
Jung S, Hoernes S, Mezger K (2001) Trace element and isotopic (Sr, Nd, Pb, O) arguments for a mid crustal origin of Pan-African garnet-bearing S-type granites from the Damara orogen (Namibia). Precambrian Res 110:325–355
Jung S, Hoernes S, Mezger K (2002) Petrology of basement-dominated terranes: II. Contrasting isotopic (Sr, Nd, Pb and O) signatures of basement-derived granites and constraints on the source region of granite (Damara orogen, Namibia). Chem Geol (submitted)
Kasch KW (1983) Continental collision, suture progradation and thermal relaxation: a plate tectonic model for the Damara orogen in central Namibia. Spec Publ Geol Soc S Africa 11:423–429
Kistler RW, Cappell BW, Peck DL, Bateman PC (1986) Isotopic variations in the Tuolumne Intrusive Suite, central Sierra Nevada, California. Contrib Mineral Petrol 94:205–220
Kröner A (1982) Rb/Sr geochronology and tectonic evolution of the Pan-African Damara belt of Namibia, southwestern Africa. Am J Sci 282:1471–1507
Kukla C, Kramm U, Kukla PA, Okrusch M (1991) U–Pb monazite data relating to metamorphism and granite intrusion in the northwestern Khomas Trough, Damara Orogen, central Namibia. Comm Geol Surv Namibia 7:49–54
LeBel L, Cocherie A, Baubron, J-C, Fouillac AM, Hawkesworth, CJ (1985) A high K, mantle-derived plutonic suite from 'Linga', near Arequipa, Peru. J Petrol 26:124–148
Lechler PJ, Desilets MO (1987) A review of the use of loss on ignition as a measure of total volatiles in whole rock analysis. Chem Geol 63:341–344
Le Fort P, Cuney M, Deniel C, France-Lanord C, Sheppard SMF, Upreti BN, Vidal P (1987) Crustal generation of the Himalayan leucogranites. Tectonophysics 134:39–57
Masberg HP, Hoffer E, Hoernes S (1992) Microfabrics indicating granulite-facies metamorphism in the low-pressure central Damara Orogen, Namibia. Precambrian Res 55:243–257
Mattinson JM (1986) Geochronology of high pressure–low temperature Franciscan metabasites. A new approach using the U–Pb system. Geol Soc Am Mem 164:95–105
McDermott F, Harris NBW, Hawkesworth CJ (1996) Geochemical constraints on crustal anatexis: a case study from the Pan-African granitoids of Namibia. Contrib Mineral Petrol 123:406–423
Mezger K, Rawnsley CM, Bohlen SR, Hanson GN (1991) U–Pb garnet, sphene, monazite, and rutile ages,: implications for the duration of high-grade metamorphism and cooling histories, Adirondack Mts, New York. J Geol 99:415–428
Mezger K, Essene EJ, van der Pluijm BA, Halliday AN (1993) U–Pb geochronology of the Grenville orogen of Ontario and New York; constraints on ancient crustal tectonics. Contrib Mineral Petrol 114:13–26
Michard A, Guiret P, Soudant M, Albarède F (1985) Nd isotopes in French Phanerozoic shales: external vs. internal aspects of crustal evolution. Geochim Cosmochim Acta 49:601–610
Miller RMG (1983) The Pan-African Damara Orogen of South West Africa/Namibia. Spec Publ Geol Soc S Afr 11:431–515
Noyes HJ, Wones DR, Frey FA (1983) A tale of two plutons: geochemical evidence bearing on the origin and differentiation of the Red Lake and Eagle Peak plutons, central Sierra Nevada, California. J Geol 91:487–509
Perfit MR, Gust DA, Bence AE, Arculus RJ, Taylor SR (1980) Chemical characteristics of island arc basalts: implications for mantle sources. In: LeMaitre RW, Cundari A (eds) Chemical characterization of tectonic provinces. Chem Geol 30:227–256
Petford N, Atherton M (1996) Na-rich partial melts from newly underplated basaltic crust: the Cordillera Blanca batholith, Peru. J Petrol 37:1491–1521
Petford N, Gallagher K (2001) Partial melting of mafic (amphibolitic) lower crust by periodic influx of basaltic magma. Earth Planet Sci Lett 193:483–499
Pidgeon RT, Bosch D, Bruguier O (1996) Inherited zircon and titanite U–Pb systematics in an Archean syenite from southwestern Australia: implications for U–Pb stability of titanite. Earth Planet Sci Lett 141:187–198
Pitcher WS (1978) Anatomy of a batholith. J Geol Soc Lond 135:157–182
Pitcher WS (1987) Granites and yet more granites forty years on. Geol Rundsch 76:51–79
Puhan D (1983) Temperature and pressure of metamorphism in the Central Damara orogen. Spec Publ Geol Soc S Afr 11:219–223
Rapp RP, Watson EB (1995) Dehydration melting of metabasalt at 8–32 kbar: implications for continental growth and crust-mantle recycling. J Petrol 36:891–932
Rapp RP, Watson EB, Miller CF (1991) Partial melting of amphibolite/eclogite and the origin of Archaean trondhjemites and tonalites. Precambrian Res 51:1–25

Reid JB (1983) Magma mixing in granitic rocks of the central Nevada, California. Earth Planet Sci Lett 66:243–261
Reiners PW, Nelson BK, Ghiorso MS (1995) Assimilation of felsic crust by basaltic magma: thermal limits and extents of crustal contamination of mantle-derived magmas. Geology 23:563–566
Roberts MP, Clemens JD (1993) origin of high-potassium, calc-alkaline, I-type granitoids. Geology 21:825–828
Rollinson HR (1993) Using geochemical data: evaluation, presentation, interpretation. Longman, London
Rushmer T (1991) Partial melting of two amphibolites: contrasting experimental results under fluid absent conditions. Contrib Mineral Petrol 107:41–59
Rutter MJ, Wyllie PJ (1988) Melting of vapour-absent tonalite at 10 kbar to simulate dehydration-melting in the deep crust. Nature 331:159–160
Saunders AD, Tarney J, Weaver SD (1980) Transverse geochemical variations across the Arctic peninsula: implications for the genesis of calc-alkaline magmas. Earth Planet Sci Lett 46:344–360
Scott DJ, St-Onge MR (1995) Constraints on Pb closure temperature in sphene based on rocks from the Ungava orogen, Canada: implications for geochronology and P–T–t path determinations. Geology 23:1123–1126
Shaw A, Downes H, Thirlwall MF (1993) The quartz diorites of Limousin: elemental and isotopic evidence for Devono-Carboniferous subduction in the Hercynian belt of the French Massif Central. Chem Geol 107:1–18
Stacey JS, Kramers JD (1975) Approximation of terrestrial lead isotope evolution by a two-stage model. Earth Planet Sci Lett 26:207–221
Taylor SR, McLennan SM (1985) The continental crust: its composition and evolution. Blackwell Science, London
Tepper JH, Nelson BK, Bergantz GW, Irving AJ (1993) Petrology of the Chiliwack batholith, North Cascades, Washington: generation of calc-alkaline granitoids by melting of mafic lower crust with variable water fugacity. Contrib Mineral Petrol 113:333–351
Thirlwall MF, Graham AM (1984) Evolution of high-Ca, high-Sr C-series basalts from Grenada, lesser Antilles: the effects of intra-crustal contamination. J Geol Soc Lond 141:427–445
Tucker RD, Raheim A, Krogh TE, Corfu F (1986) Uranium–lead zircon and titanite ages from the northern portion of the Western Gneiss Region, south-central Norway. Earth Planet Sci Lett 81:203–211
Verts LA, Chamberlain KR, Frost CD (1996) U–Pb sphene dating of metamorphism: the importance of sphene growth in the contact aureole of the Red Mountain pluton, Laramie Mountains, Wyoming. Contrib Mineral Petrol 125:186–199
Wareham CD, Vaughan APM, Millar IL (1997) The Wiley Glacier complex, Antarctic Peninsula: pluton growth by pulsing of granitoid magmas. Chem Geol 143:65–80
Wolf MB, Wyllie PJ (1993) Garnet growth during amphibolite anatexis: implications of a garnetiferous restite. J Geol 101:357–373
Wolf MB, Wyllie PJ (1994) Dehydration-melting of amphibolite at 10 kbar: the effects of temperature and time. Contrib Mineral Petrol 115:369–383
Zhang LS, Schärer U (1996) Inherited Pb components in magmatic titanite and their consequences for the interpretation of U–Pb ages. Earth Planet Sci Lett 138:57–65